

NEAR: A Training-Free Pre-Estimator of Machine Learning Model Performance

Raphael T. Husistein, Markus Reiher,* and Marco Eckhoff†
ETH Zurich, Department of Chemistry and Applied Biosciences,
Vladimir-Prelog-Weg 2, 8093 Zurich, Switzerland.

(Dated: August 16, 2024)

Artificial neural networks have been shown to be state-of-the-art machine learning models in a wide variety of applications, including natural language processing and image recognition. However, building a performant neural network is a laborious task and requires substantial computing power. Neural Architecture Search (NAS) addresses this issue by an automatic selection of the optimal network from a set of potential candidates. While many NAS methods still require training of (some) neural networks, zero-cost proxies promise to identify the optimal network without training. In this work, we propose the zero-cost proxy *Network Expressivity by Activation Rank* (NEAR). It is based on the effective rank of the pre- and post-activation matrix, i.e., the values of a neural network layer before and after applying its activation function. We demonstrate the cutting-edge correlation between this network score and the model accuracy on NAS-Bench-101 and NATS-Bench-SSS/TSS. In addition, we present a simple approach to estimate the optimal layer sizes in multi-layer perceptrons. Furthermore, we show that this score can be utilized to select hyperparameters such as the activation function and the neural network weight initialization scheme.

Keywords: Network Expressivity by Activation Rank (NEAR), Effective Rank, Neural Architecture Search

1. INTRODUCTION

Originally inspired by the structure and function of biological neural networks, artificial neural networks are now a key component in machine learning [1, 2]. They are applied in many tasks such as natural language processing, speech recognition, and even protein folding [3–5]. Artificial neural networks are built by layers of interconnected neurons, which receive inputs, apply a, typically non-linear, activation function, and pass on the result (see Figure 1). By tuning the weights of the individual inputs to a neuron, a neural network can learn functional relations from sample data to perform predictions without explicit program instructions. Deep learning is obtained if more than one layer is hidden between the first input and last output layer of the neural network. In theory, already a neural network with a single hidden layer and enough neurons is capable of approximating any continuous function up to arbitrary precision [6–8].

However, the choice of the model size, i.e., the number of hidden layers and the number of neurons per layer, has a huge impact on the performance, training time, and computational demand [9]. A too small network is unable to capture a complex relation in a dataset resulting in underfitting. Conversely, a too large model lacks efficiency and carries the risk of overfitting and poor generalization. Determining the optimal model size that strikes a balance between accuracy and efficiency remains an important challenge [10]. In common practise, various models of different sizes are trained and their final performances are compared. This manual process is time-consuming and often leads to sub-optimal model architectures.

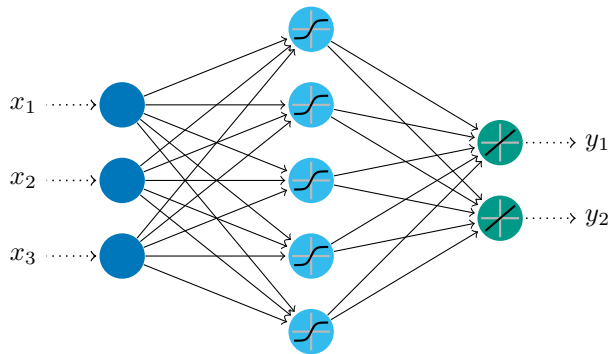


Figure 1: Illustration of an artificial neural network with three inputs $\{x_i\}$ and two outputs $\{y_i\}$. The single hidden layer consists of five neurons. The activation functions are shown within the neurons. The solid lines represent the weights, while the dashed lines indicate input and output without weights.

The goal of Neural Architecture Search (NAS) is to eliminate this manual process and autonomously identify suitable architectures [11]. Commonly applied techniques for NAS are based on reinforcement learning, evolutionary algorithms, or gradient-based optimization [12–14]. However, these methods are still time- and resource-intensive. Zero-cost proxies have been proposed to improve the efficiency of NAS methods [15–17]. They exploit properties of the untrained network that are correlated with the final accuracy, bypassing the costly training process. In this way, they promise speed-ups of several orders of magnitude compared to traditional NAS algorithms [16]. The performance of previously reported zero-cost proxies is highly dependent on the underlying search space [18]. Furthermore, many of them are unable to demonstrate consistently a higher correlation with the final accuracy than the trivial baseline given by the number of param-

* mreiher@ethz.ch
† eckhoffm@ethz.ch

ters (#Params) [18]. In addition, these proxies require a search space of known architectures. While the latter is not a severe limitation in applications such as computer vision, in many other applications such search spaces do not exist. An example is a so-called machine learning potential [19, 20] applied in chemistry and materials science, which employs neural networks to predict the energy of a chemical system as a function of the molecular structure. In this work, we propose the zero-cost proxy *Network Expressivity by Activation Rank* (NEAR) that can be used in conjunction with a search space, but also provides the possibility to estimate the optimal layer size for multi-layer perceptrons without a search space.

Besides the network architecture, the activation function and weight initialization scheme have a significant impact on the training dynamics and the final performance of a neural network [21, 22]. A variety of techniques have been developed to select such hyperparameters, including methods based on Bayesian optimization and evolutionary algorithms [23, 24]. However, these techniques still require expensive training of multiple networks, and the zero-cost proxies reported so far have not been applied to the selection of the activation function and the weight initialization scheme. A zero-cost proxy that can be applied not only to find optimal architectures, but also to choose the activation function and the weight initialization scheme, would allow one to further reduce the computational burden of constructing a performant artificial neural network. Here, we therefore evaluate the suitability of our zero-cost proxy NEAR for this purpose. In summary, we make the following key contributions:

- We propose the zero-cost proxy NEAR and test its performance across several search spaces and datasets.
- We introduce a simple method to estimate the optimal layer size of multi-layer perceptrons and show its effectiveness for machine learning potentials.
- We empirically demonstrate that our zero-cost proxy NEAR can support the selection of an activation function and a suitable weight initialization scheme.

This work is organized as follows: In Section 2, we discuss previously introduced zero-cost proxies. In Section 3, we show how the effective rank previously published in Ref. [25] can be employed to construct a zero-cost proxy. We evaluate the performance of our zero-cost proxy NEAR on several benchmarks in Section 4. Further, we show that NEAR can detect not only optimal architectures in a search space, but also estimate optimal layer sizes in multi-layer perceptrons. Additionally, in Section 4 we demonstrate that NEAR can be applied to choose performant activation functions and weight initializations. Conclusions are then given in Section 5.

2. RELATED WORK

Zero-cost NAS proxies are designed to identify optimal neural network architectures without requiring training. Some of the earliest proxies such as *Single-Shot Network Pruning Based on Connection Sensitivity* (SNIP), *Gradient Signal Preservation* (GraSP), Fisher, and *Synaptic Flow* (SynFlow) have been adapted from pruning techniques and are based on gradients of the neural network [16]. While SNIP assigns scores to individual parameters by approximating the change in loss when the parameter is removed [26], the scores of GraSP are based on an approximation of the change in the gradient norm [27]. The Fisher proxy estimates the importance of an activation by calculating its contribution to the loss [28], and SynFlow assigns a score to each parameter indicating how much it contributes to the information flow in the network [29]. A proxy that has not been adapted from the pruning literature is Grad_norm, which is defined as the Euclidean norm of the gradient [16]. SNIP, GraSP, SynFlow, and Grad_norm are calculated for each individual parameter, whereas Fisher is calculated for channels within a convolution layer. To obtain a score for the entire network, the values assigned to the parameters or channels are summed. *Zero-Shot NAS via Inverse Coefficient of Variation on Gradients* (ZiCo) [30] is another proxy that exploits gradient information, linking the mean and the variance of the gradient to the convergence rate and the capacity of the neural network. With the exception of SynFlow, all the aforementioned proxies require the presence of target output, so-called labels. Therefore, they can only be applied to a limited extent in unsupervised learning for categorization tasks.

Some zero-cost proxies exist that employ properties of the untrained network that do not require backpropagation and hence work without labels. These include *Neural Architecture Search Without Training* (NASWOT) [15], Zen-Score [31], *Sample-Wise Activation Patterns* (swap) [32], *Regularized Sample-Wise Activation Patterns* (reg_swap) [32], and *Minimum Eigenvalue of Correlation* (MeCo_{opt}) [33]. To a certain extent, these proxies can be related to theoretical considerations regarding, for example, the functions that can be represented by a particular neural network or the convergence rate during training. A proxy that combines information from gradients with the output of the untrained network and works without labels is *Training-Free Neural Architecture Search* (TE-NAS) [34].

All these proxies assess the performance of a network based on the output of individual untrained layers. However, most of them, namely NASWOT, Zen-Score, swap, reg_swap, and TE-NAS, can only be applied if the Rectified Linear Unit (ReLU) [35] activation function is employed. Our zero-cost proxy NEAR utilizes the output of individual layers before and after the application of the activation function for sample inputs without constraints on the type of activation function. Therefore, its applicability is more general.

3. METHODS

3.1. Multi-Layer Perceptron

An artificial neural network with the architecture described in the introduction (see Figure 1) is also called multi-layer perceptron. A multi-layer perceptron with L layers can be expressed as

$$\mathcal{F}(\mathbf{x}) = (\sigma \circ \mathbf{W}_L) \circ (\sigma \circ \mathbf{W}_{L-1}) \circ \dots \circ (\sigma \circ \mathbf{W}_2) \circ (\sigma \circ \mathbf{W}_1)(\mathbf{x}) := \mathbf{y}, \quad (1)$$

where \mathbf{x} and \mathbf{y} are the input and output features, σ is an activation function, and $\mathbf{W}_l \in \mathbb{R}^{N_l \times N_{l-1}}$ are the weights of layer l . The weights can also include so-called bias weights, which are added to the output of the neuron without being multiplied by any input value. Hence, they effectively shift the activation function input of the neuron.

We define the pre-activation of layer l as

$$\mathbf{z}_l = (\mathbf{W}_l) \circ (\sigma \circ \mathbf{W}_{l-1}) \circ \dots \circ (\sigma \circ \mathbf{W}_2) \circ (\sigma \circ \mathbf{W}_1)(\mathbf{x}) \quad (2)$$

and the post-activation as

$$\mathbf{h}_l = \sigma(\mathbf{z}_l). \quad (3)$$

3.2. Network Expressivity by Activation Rank (NEAR)

The construction of our zero-cost proxy NEAR is inspired by theoretical considerations on machine learning that attempt to assess the expressivity of artificial neural networks [36, 37]. Therefore, we restate here the most important concepts from these works. For neural networks applying the ReLU activation function, each activation function can be conceptualized as a hyperplane that separates the input space into an active and an inactive region. Both regions are referred to as linear regions. The number of such linear regions can be viewed as a measure of the expressivity of the network [36, 37]. Following previous studies [38–40], we define the activation pattern for an input \mathbf{x} and a network \mathcal{F} with the ReLU activation function by the set of vectors $\mathcal{A}(\mathbf{x}; \mathcal{F}) = \{\mathbf{a}_1, \dots, \mathbf{a}_L\}$ where $a_{li} = 1$ if the output of the i th neuron in layer l is positive and $a_{li} = 0$ otherwise. Given that different linear regions correspond to distinct activation patterns, the number of linear regions is equivalent to the number of activation patterns. Consequently, it is a natural idea to analyze the activation patterns to assess the expressivity of a network. This idea is exploited in several zero-cost proxies [15, 31, 32, 34]. However, constructing a proxy based on the aforementioned definition of the activation pattern will restrict its application to networks applying the ReLU activation function, a drawback that all those proxies have in common.

To build a more general zero-cost proxy, we relax the definition of the activation pattern to enable other activation functions: $\mathcal{A}(\mathbf{x}; \mathcal{F}) = \{\mathbf{h}_1, \dots, \mathbf{h}_L\}$, with \mathbf{h}_l defined in Eq. (3). While there is no longer a direct relationship to the number of linear regions, we argue that inputs with a very similar activation pattern are more challenging for the network to distinguish, and we leverage this argument to develop our zero-cost proxy. We define the pre-activation matrix for layer l as $\mathbf{Z}_l \in \mathbb{R}^{n_l \times n_l}$, where n_l is the number of neurons in layer l . Each of the n_l rows of \mathbf{Z}_l contains \mathbf{z}_l for some different sample input \mathbf{x}_i . In a similar manner, the post-activation matrix for layer l is defined as $\mathbf{H}_l \in \mathbb{R}^{n_l \times n_l}$, where each row contains \mathbf{h}_l for a different sample input \mathbf{x}_i . Intuitively, we would expect a well-performing network when the rows in the pre-/post-activation matrix are very different to each other, while a matrix with all similar rows would indicate a poorly performing network. As an example, we can consider a classification problem in which rows are highly similar yet belong to inputs of different classes. In this case even a minor perturbation can result in a change in the predicted class. Additionally, we would expect that a matrix, in which certain rows have entries that are much larger than the entries in other rows, will result in poorer performance than a matrix with entries of similar size. The reason for this behavior is that the differences in size can cause the predictions to become highly dependent on individual weights and hence on individual input values. These two relationships are captured by the effective rank, defined as follows:

Definition 3.1 Effective Rank [25]. *The effective rank of a matrix $\mathbf{A} \in \mathbb{C}^{M \times N}$, with $Q = \min\{M, N\}$, is given by*

$$\text{erank}(\mathbf{A}) = \exp[H(p_1, \dots, p_Q)], \quad (4)$$

where $H(p_1, \dots, p_Q)$ is the Shannon entropy [41],

$$H(p_1, \dots, p_Q) = - \sum_{k=1}^Q p_k \log(p_k), \quad (5)$$

and p_k are normalized singular values,

$$p_k = \frac{\tilde{\sigma}_k}{\sum_{i=1}^Q \tilde{\sigma}_i}, \quad (6)$$

with the singular values $\tilde{\sigma}_i$.

In order to interpret the effective rank of a matrix, we can think of the matrix as a linear transformation. The rank of the matrix indicates the number of dimensions of its range. By contrast, the effective rank contains information about the geometrical shaping of the transformation. A linear transformation that causes a strong stretching along one dimension, while all other dimensions remain unchanged, has a lower effective rank than a transformation that causes an equally strong stretching along all dimensions. The rank of the matrix of both transformations is, however, identical. In addition, a linear

transformation that stretches each dimension equally is represented by a matrix with orthogonal rows, and rows that are orthogonal to each other could be considered maximally different. In other words, the effective rank measures what we have intuitively explained above as being indicators of good performance. Consequently, we propose the zero-cost proxy NEAR as the following:

Definition 3.2 Network Expressivity by Activation Rank (NEAR). *The NEAR score of a neural network is given by*

$$s = \sum_{l=1}^L \text{erank}(\mathbf{Z}_l) + \text{erank}(\mathbf{H}_l),$$

where \mathbf{Z}_l and \mathbf{H}_l denote the pre- and post-activation matrices, respectively.

A higher NEAR score s indicates a better performing network. The calculated score depends on the input samples, which will usually be randomly selected. To prevent large, random fluctuations depending on the selected samples, we recommend to calculate the score multiple times and employ the average. On the NAS benchmarks, we calculated the average of 32 repetitions, while for the machine learning potential benchmarks, we employed 400 repetitions due to the more diverse dataset.

3.3. NEAR for Convolutional Neural Networks

Convolutional Neural Networks (CNNs) are a neural network architecture particularly popular in the field of computer vision [42]. Our description here focuses on networks applying 2D convolutions. However, the approach can be extended to 3D convolutions as well. For 2D convolutions, the input has the dimensions $W \times H \times C$, where C is the number of channels. For example, C equals 3 for color images, since these consist of red, green, and blue color channels with dimension $W \times H$ (number of pixels in width W and height H). To extract features from the input, a convolution operation is performed (see Figure 2) using one or more filters with dimension $k \times k \times C$, where k is an adjustable hyperparameter. These filters are essentially the weights that are learned during the training process. The results of the convolutions are summed, so that each filter results in a single output matrix, also known as a feature map. The output is passed to the next layer, where new filters are applied, allowing the network to learn increasingly complex features.

We employ the feature maps in the construction of the activation matrix to calculate the NEAR score for a CNN. A layer with C input channels results in an output of the form $\mathbf{Z}_l \in \mathbb{R}^{W' \times H' \times C'}$, with $W' = W - k + 1$ and $H' = H - k + 1$ (in case of no padding and stride of one). C' denotes the number of filters in the layer. Since this output is a 3D tensor, the NEAR score cannot be calculated directly. Instead, the output is first transformed into a matrix. We consider the number of filters

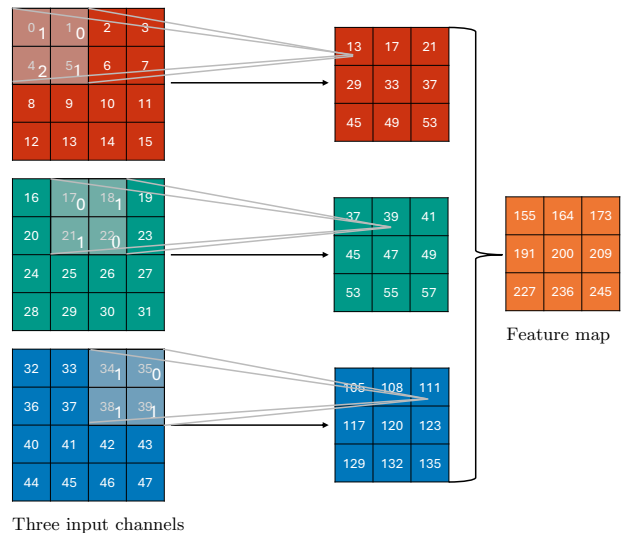


Figure 2: A convolution is performed on the input of dimension $4 \times 4 \times 3$ with a filter of dimension $2 \times 2 \times 3$ resulting in a feature map of dimension 3×3 .

to be analogous to the number of neurons in a fully connected layer. Therefore, the maximum possible NEAR score should be larger if there are more filters in a layer. This behavior could be achieved by flattening each feature map into a vector and then packing the vectors into a matrix. However, for an image with three channels and 32×32 pixels as input, this approach quickly results in a large matrix. For example, when using a filter of dimension $3 \times 3 \times 8$, the matrix already is of dimensions 7200×7200 , and the effort to compute the NEAR score is no longer negligible. Therefore, we approximate this matrix for the calculation of the NEAR score. First, we flatten the output to get $\mathbf{Z}_l \in \mathbb{R}^{W' \cdot H' \times C'}$ (see Figure 3). Second, to reduce the size of the first dimension of this matrix, a random selection of C' contiguous rows is made, where the first row contains elements taken from the first row of the feature maps. This approach yields essentially a submatrix of the large matrix containing all the feature maps as vectors. We employ this submatrix as a proxy to compute the NEAR score.

4. RESULTS AND DISCUSSION

4.1. Correlation of Effective Rank and Final Model Accuracy

To examine the performance of our zero-cost proxy NEAR, we evaluated it on the three standard cell-based NAS benchmarks NAS-Bench-101 [43], NATS-Bench-SSS, and NATS-Bench-TSS [44]. We note that “cell-based” refers to the construction of the individual networks, which were obtained by placing stacks of repeated cells in a common skeleton (for details see Refs. [43] and [44]). For comparison, we report the two commonly em-

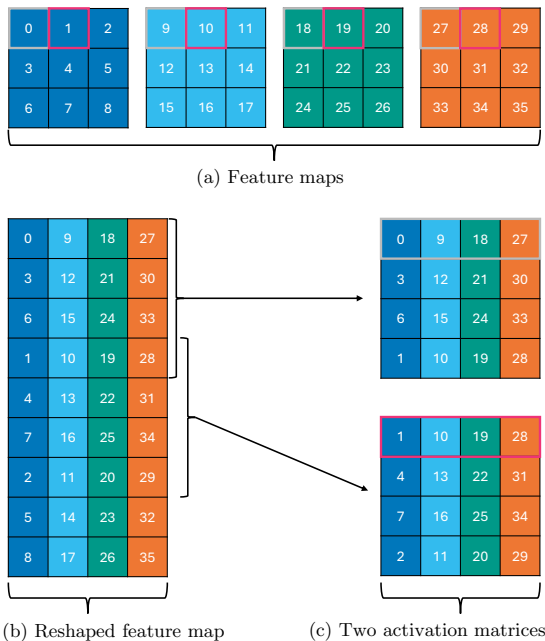


Figure 3: Process of reshaping convolutional neural network feature maps. (a) The process begins with four 3×3 feature maps. (b) These feature maps are subsequently reshaped to a 9×4 matrix. (c) An activation matrix is given by four contiguous rows, whereby the first row contains elements extracted from the top row of the feature maps. From all possible activation matrices one is randomly selected.

ployed rank correlation measures Kendall’s τ [45] and Spearman’s ρ [46] also for twelve other zero-cost proxies. For Grad_norm, SNIP, GraSP, Fisher, and SynFlow we relied on the implementations of Ref. [16] and for ZiCo [30], MeCo_{opt} [33], swap [32], and reg_swap [32] we employed the respective paper’s implementation. All results were recalculated by us. In some cases we observed small differences in the correlation coefficients compared to the values of the original publications. To make our calculations reproducible, the code including all hyperparameter settings is available on Zenodo [47].

NATS-Bench-TSS

The NATS-Bench-TSS search space consists of 15 625 neural network architectures trained on the datasets CIFAR-10, CIFAR-100 [48], and ImageNet16-120 [49]. The correlation between the different proxies and the final test accuracy is shown in Table 1. Some of the previously reported proxies, such as Grad_norm, SNIP, and GraSP, yield a lower correlation than the number of parameters. The latter can be seen as trivial baseline for the zero-cost proxies. The more recently developed proxies ZiCo, MeCo_{opt}, swap, reg_swap, and our proxy NEAR demonstrate superior performance relative

to this baseline. In general, MeCo_{opt} achieves the highest correlation across all datasets for NATS-Bench-TSS. Nevertheless, the NEAR and reg_swap results are very close to those of MeCo_{opt}. However, the comparison to the reg_swap score is not entirely fair because it assumes that architectures with a parameter number close to the chosen parameter μ perform best, which may not be universally true. MeCo_{opt} and NEAR are therefore more generally applicable.

Table 1: Kendall’s τ and Spearman’s ρ correlation coefficients for different zero-cost proxies on the NATS-Bench-TSS benchmark. The highest correlation is highlighted in bold face.

NATS-Bench-TSS						
Dataset	CIFAR-10		CIFAR-100		IN16-120	
Proxy	Correlation					
	τ	ρ	τ	ρ	τ	ρ
Grad_norm [16]	0.48	0.65	0.47	0.64	0.41	0.56
SNIP [16]	0.48	0.64	0.47	0.63	0.43	0.57
GraSP [16]	0.39	0.55	0.40	0.57	0.40	0.55
Fisher [16]	0.41	0.55	0.41	0.56	0.35	0.47
SynFlow [16]	0.58	0.77	0.57	0.76	0.49	0.67
Zen-Score [31]	0.32	0.43	0.31	0.42	0.32	0.44
FLOPs	0.58	0.75	0.55	0.73	0.51	0.68
#Params	0.58	0.75	0.55	0.73	0.49	0.66
ZiCo [30]	0.58	0.78	0.60	0.80	0.57	0.76
MeCo _{opt} [33]	0.72	0.90	0.73	0.90	0.67	0.84
swap [32]	0.64	0.82	0.65	0.82	0.58	0.74
reg_swap [32]	0.71	0.88	0.69	0.87	0.62	0.79
NEAR	0.70	0.88	0.69	0.87	0.66	0.84

NATS-Bench-SSS

For the larger NATS-Bench-SSS search space with 32 768 architectures trained on CIFAR-10, CIFAR-100, and ImageNet16-120, neither MeCo_{opt} nor reg_swap consistently show a higher correlation with the final test accuracy than the number of parameters (Table 2). Only SynFlow, NEAR, and ZiCo are able to surpass the performance of this baseline on all three datasets, with SynFlow demonstrating the highest correlation on CIFAR-10 and ImageNet16-120, and NEAR yielding the highest correlation on CIFAR-100.

NAS-Bench-101

The NAS-Bench-101 search space consists of 423 624 architectures trained on the CIFAR-10 dataset. As shown in Table 3, NEAR achieves the highest correlation with the final accuracy for both metrics. It significantly outperforms MeCo_{opt}, SynFlow, and reg_swap, which show competitive performance on NATS-Bench-TSS and NATS-Bench-SSS. The second highest correlation for NAS-Bench-101 is shown by the Zen-Score, closely fol-

Table 2: Kendall’s τ and Spearman’s ρ correlation coefficients for different zero-cost proxies on the NATS-Bench-SSS benchmark. The highest correlation is highlighted in bold face.

NATS-Bench-SSS						
Dataset	CIFAR-10		CIFAR-100		IN16-120	
Proxy \ Correlation	τ	ρ	τ	ρ	τ	ρ
Grad_norm [16]	0.53	0.72	0.38	0.54	0.52	0.70
SNIP [16]	0.63	0.82	0.43	0.61	0.61	0.79
GraSP [16]	0.30	0.43	0.10	0.15	0.33	0.48
Fisher [16]	0.47	0.65	0.30	0.43	0.43	0.60
SynFlow [16]	0.79	0.94	0.59	0.78	0.81	0.95
Zen-Score [31]	0.75	0.92	0.50	0.69	0.72	0.89
FLOPs	0.44	0.61	0.19	0.28	0.41	0.57
#Params	0.69	0.87	0.53	0.72	0.68	0.86
ZiCo [30]	0.72	0.89	0.54	0.74	0.73	0.90
MeCo _{opt} [33]	0.74	0.91	0.62	0.81	0.61	0.80
swap [32]	0.48	0.67	0.23	0.34	0.43	0.60
reg_swap [32]	0.62	0.81	0.38	0.54	0.55	0.73
NEAR	0.74	0.91	0.62	0.82	0.76	0.92

lowed by ZiCo. However, Zen-Score yields worse correlation than the number of parameters on NATS-Bench-TSS across all datasets.

Table 3: Kendall’s τ and Spearman’s ρ correlation coefficients for different zero-cost proxies on the NAS-Bench-101 benchmark. The highest correlation is highlighted in bold face.

NAS-Bench-101		
Proxy \ Correlation	τ	ρ
Grad_norm [16]	-0.17	-0.25
SNIP [16]	-0.12	-0.17
GraSP [16]	0.17	0.25
Fisher [16]	-0.19	-0.28
SynFlow [16]	0.25	0.37
Zen-Score [31]	0.47	0.64
FLOPs	0.30	0.43
#Params	0.30	0.43
ZiCo [30]	0.45	0.63
MeCo _{opt} [33]	0.35	0.49
swap [32]	0.31	0.43
reg_swap [32]	0.30	0.43
NEAR	0.52	0.70

Summary

To compare the performance of the zero-cost proxies across all datasets and search spaces, we provide a ranking. For each combination of search space and dataset, we order the zero-cost proxies according to their Spearman’s ρ value. We identify the position in this order as rank, whereby the proxy of highest correlation is assigned a rank of one. Subsequently, the average over all

datasets for each NAS search space and for all search spaces is calculated. For example, NEAR achieves ranks three, one, and two on NATS-Bench-SSS for CIFAR-10, CIFAR-100, and ImageNet16-120, respectively. These rankings result in an average rank of two on this search space. Of the proxies tested, reg_swap, SynFlow, ZiCo, MeCo_{opt}, and NEAR are on average better than the baseline given by the number of parameters (Table 4). However, only NEAR and ZiCo yield consistently higher correlation than the number of parameters for each combination of search space and dataset, whereby NEAR outperforms ZiCo in every case. For each search space, NEAR is either the best or second best zero-cost proxy highlighting its broad applicability. Overall, NEAR achieves the best rank, followed by MeCo_{opt} and ZiCo.

Table 4: The rank of different zero-cost proxies averaged over all datasets of NATS-Bench-TSS, NATS-Bench-SSS, and NAS-Bench-101 and across all search spaces. The best rank is highlighted in bold face.

Average rank					
Proxy	Search space	TSS	SSS	101	All
	GraSP [16]	9.33	12.00	7.00	10.14
Fisher [16]	10.00	9.67	10.00	9.86	
Grad_norm [16]	7.67	8.33	9.00	8.14	
FLOPs	5.67	11.00	5.00	7.86	
SNIP [16]	8.00	6.67	8.00	7.43	
Zen-Score [31]	11.00	4.00	2.00	6.71	
swap [32]	3.33	9.67	5.00	6.29	
#Params	6.33	5.00	5.00	5.57	
reg_swap [32]	2.00	7.67	5.00	4.86	
SynFlow [16]	5.33	1.67	6.00	3.86	
ZiCo [30]	3.67	3.67	3.00	3.57	
MeCo _{opt} [33]	1.00	3.67	4.00	2.57	
NEAR	1.67	2.00	1.00	1.71	

4.2. Estimation of Optimal Layer Size

Inspired by previous work that suggested a power law scaling for the accuracy with respect to the model size for language models [50], we analyzed the NEAR score of a single layer of different sizes. We observed that the relative score, i.e., the score divided by the number of neurons, appears to be well represented by a simple power function of the form $f(s) = \alpha + \beta \cdot s^\gamma$, where s is the NEAR score (see Figure 4). This behavior is consistent for two different datasets. One is the balanced version of the extended MNIST (EMNIST) dataset [51]. It contains handwritten digits and letters, with an equal number of examples for each class. It is therefore more challenging than the original MNIST dataset including only digits [52]. The other is a molecular dataset for a lifelong machine learning potential. This dataset includes target energies and atomic forces for features given by molecular structures. These molecular structures were obtained

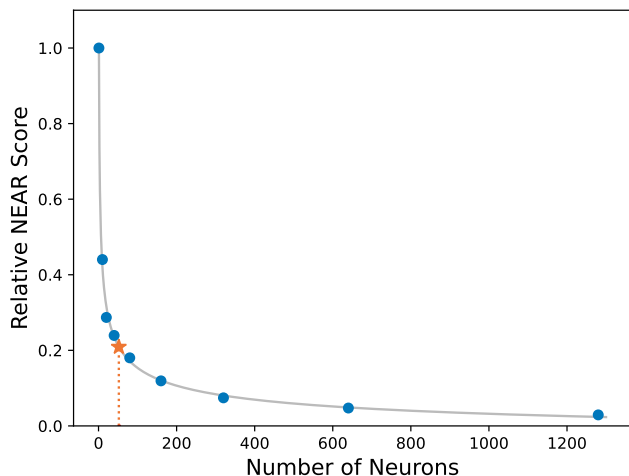


Figure 4: A power function fitted to the NEAR score divided by the total number of neurons in the layer. The star marks the first time where the slope is smaller or equal to 0.5% of the slope at $x = 1$. The plot has been generated for the experiments on the machine learning potential.

from various conformations in 42 different S_N2 reactions (8 600 structures) [53].

We argue that a decreasing relative NEAR score indicates that the network benefits less from additional neurons and, at a certain threshold, its performance is no longer limited by its size. Our experiments suggest a threshold based on the slope of the power function to work reasonably well. We therefore propose the following approach to estimate the size of individual layers:

1. Calculate the NEAR score for some different layer sizes.
2. Fit a power function to the calculated relative scores.
3. Calculate at which layer size the slope of the fit falls below a certain threshold and apply this layer size for the neural network.

Since the NEAR score of each layer depends only on the previous layers, this approach can also be applied to networks with multiple layers. Starting with the first layer, the size of all layers can be determined iteratively.

Machine Learning Potential

We applied our approach to estimate the layer sizes on a three-hidden-layer lifelong machine learning potential, employing the dataset B of Ref. [53]. Our method predicted a size of 52, 58, and 60 for the first, second, and third hidden layers, respectively, with a threshold of 0.5% of the slope at a layer size of 1. These sizes are significantly smaller than applied in Ref. [53] (which are 102, 61, and 44). While this change reduces the number of parameters from 22 990 to 13 909,

the average test loss only increases from 0.012 ± 0.003 to 0.015 ± 0.004 . This increase is reflected in a change of the root mean squared error for the energies from $(4.4 \pm 1.2) \text{ meV atom}^{-1}$ to $(4.6 \pm 1.2) \text{ meV atom}^{-1}$ and for the forces from $(100 \pm 8) \text{ meV \AA}^{-1}$ to $(109 \pm 8) \text{ meV \AA}^{-1}$. These numbers represent the mean and standard deviation over 20 individual lifelong machine learning potentials, for which the training was started from different randomly initialized neural networks. We note that the test loss depends not only on the capacity of the neural network, but also on the training process. However, NEAR only aims to capture the capacity of a network and does not take into account the training dynamics. Therefore, NEAR alone cannot be expected to determine the perfect size but rather to give a good estimate.

Keeping the size of the first and second hidden layers at 52 and 58, respectively, and only varying the size of the third hidden layer showed that the predicted size achieves good performance. Even increasing the layer size to 100 neurons did not improve the loss (Table 5). However, a slightly smaller layer of 40 neurons would still be sufficient to achieve the same performance. Another point to note here is that smaller networks require fewer computational resources and are therefore more efficient to evaluate.

Table 5: The test loss of trained lifelong machine learning potentials with different sizes of the third hidden layer, while the first and second layers are fixed at 52 and 58 neurons, respectively. Marked in bold is the architecture predicted by our approach. All experiments were repeated 20 times with different randomly initialized neural networks. We show the mean and standard deviation (rounded up).

Layer size	Test loss	#Params
20	0.017 ± 0.003	11 509
40	0.015 ± 0.003	12 709
60	0.015 ± 0.004	13 909
80	0.014 ± 0.003	15 109
100	0.015 ± 0.003	16 309

Repeating the experiment for a variable second hidden layer showed again that the predicted size has favorable characteristics in terms of accuracy and number of parameters. Reducing the size of the second layer to 38 neurons, which corresponds to a reduction in the number of parameters by $\sim 16\%$, results in an increase in the loss of 20%. Conversely, increasing the neuron number to 78, which corresponds to an increase in the parameter number by $\sim 16\%$, yields a loss decrease of only $\sim 7\%$ (Table 6).

Balanced Extended MNIST

In a second experiment, we estimated the layer sizes for a two-hidden layer neural network on the balanced EM-

Table 6: The test loss of trained lifelong machine learning potentials with different sizes of the second hidden layer, while the first and third layers are fixed at 52 and 60 neurons, respectively. Marked in bold is the architecture predicted by our approach. All experiments were repeated 20 times with different randomly initialized neural networks. We show the mean and standard deviation (rounded up).

Layer size	Test loss	#Params
18	0.022 ± 0.004	9 389
38	0.018 ± 0.004	11 649
58	0.015 ± 0.004	13 909
78	0.014 ± 0.004	16 169
98	0.014 ± 0.003	18 429

NIST dataset. Again, we applied a threshold of 0.5% of the slope at a layer size of 1. The resulting sizes were 200 for both, first and second hidden layer. A comparison of the test loss to a network with a reduced second layer size of 120, which decreases the parameter number by $\sim 10\%$, shows an loss increase of $\sim 4\%$. The aforementioned loss values correspond to a classification accuracy of 86.85% and 87.30%. Conversely, an increase in the neuron number to 280 for the second layer, which increases the parameter number by $\sim 9\%$, results in a decrease in the loss of around 1% and an increase in the accuracy to 87.34%. This observation suggests that a size of 200 represents a reasonable compromise between efficiency and accuracy (Table 7).

Table 7: The test loss on the balanced EMNIST dataset for different sizes of the second layer, while the first layer has a fixed size of 200 neurons. Marked in bold is the architecture predicted by our approach. All experiments were repeated 20 times with different randomly initialized neural networks. We show the mean and the standard deviation (rounded up).

Layer size	Test loss	#Params
40	0.433 ± 0.017	166 967
80	0.397 ± 0.011	176 887
120	0.383 ± 0.009	186 807
160	0.376 ± 0.009	196 727
200	0.368 ± 0.006	206 647
240	0.364 ± 0.006	216 567
280	0.364 ± 0.008	226 487
320	0.363 ± 0.009	236 407
360	0.359 ± 0.007	246 327

To check whether also the prediction for the first layer was reasonable, we fixed the size of the second layer to 200 and train networks with various sizes for the first layer (Table 8). A comparison of the test loss for a network with a size of 160 ($\sim 20\%$ decrease in the parameter number) yields an increase in the loss of $\sim 1.3\%$ and a decrease in the accuracy from 87.30% to 87.14%. Even when the size of the first layer was increased to 260 ($\sim 30\%$ increase in the parameter number), the loss can

only be reduced by $\sim 0.7\%$ and the accuracy is increased to 87.32%. Again, the predicted size appears to offer a good trade-off between the number of parameters and the accuracy.

Table 8: The test loss on the balanced EMNIST dataset for different sizes of the first layer, while the second layer has a fixed size of 200 neurons. Marked in bold is the architecture predicted by our approach. All experiments were repeated 20 times with different randomly initialized neural networks. We show the mean and the standard deviation (rounded up).

Layer size	Test loss	#Params
120	0.393 ± 0.012	127 847
140	0.380 ± 0.006	147 547
160	0.373 ± 0.009	167 247
180	0.368 ± 0.007	186 947
200	0.368 ± 0.006	206 647
220	0.363 ± 0.007	226 347
240	0.359 ± 0.006	246 047
260	0.366 ± 0.007	265 747

4.3. Estimation of Activation Function and Weight Initialization Performance

Numerous NAS benchmarks, including NATS-Bench-TSS, NATS-Bench-SSS, and NAS-Bench-101, apply the ReLU activation function for all networks. There is no attention for zero-cost proxies to detect favorable activation functions or weight initialization schemes. There are even proxies that are specifically designed for the ReLU activation function [15, 32, 34]. However, it is well known that choosing an appropriate activation function and weight initialization scheme is crucial for achieving good model performance [21, 22, 53]. To assess whether NEAR can be employed to select an activation function and a weight initialization scheme, we calculated the score before training and compared it with the final model performance.

Machine Learning Potential

We previously reported that the activation function $sTanh(x) = 1.59223 \cdot \tanh(x)$ with a tailored weight initialization scheme improves the final accuracy of a lifelong machine learning potential [53]. We repeated the training for the same dataset and the same neural network architecture (number of neurons per layer: 133 – 102 – 61 – 44 – 1) employing the CoRe optimizer [53–55].

Table 9 shows that the sTanh activation function with the tailored weight initialization scheme achieves the lowest test loss, while also exhibiting the largest NEAR score. Comparing the two weight initialization schemes sTanh

and Kaiming uniform [56] demonstrates that the former improves performance and that the NEAR score can be applied as a reliable predictor for the more suitable weight initialization scheme.

A comparison of the loss and NEAR score of different activation functions applying the same weight initialization scheme also shows that the score can guide the selection of an appropriate activation function. For example, the activation function sTanh with the customized initialization scheme exhibits the lowest loss and the highest NEAR score, while the activation function Tanhshrink shows the highest loss and lowest NEAR score for this weight initialization scheme. However, the discrepancies in loss for the three best activation functions sTanh, Sigmoid Linear Unit (SiLU) [57], and Tanh are minimal, whereas the differences in the NEAR score would suggest larger differences. The lowest NEAR score is obtained by Tanhshrink with Kaiming initialization, which is also consistent with the fact that this combination achieves the highest average loss. Hence, NEAR is capable of identifying more and less effective activation functions, while the ordering in close cases cannot be guaranteed. Since the loss function of the lifelong machine learning potential includes derivative constraints, the second derivative of the activation function appears in the gradient calculation. Consequently, only activation functions with a non-zero second derivative can be considered, resulting in the omission of the ReLU function in this experiment. This issue once again highlights the benefit of NEAR that it can be applied to any activation function.

Table 9: Comparison of the test loss (after training) and the NEAR score (before training) for various activation functions σ and weight initialization schemes.

The table is sorted by ascending test loss. All experiments were repeated 20 times with different randomly initialized neural networks and a random selection of inputs employed to calculate the NEAR score in each repetition. We report the mean and the standard deviation (rounded up).

σ , initialization	Test loss	NEAR score
sTanh, sTanh	0.012 ± 0.003	70.8 ± 0.2
SiLU, sTanh	0.013 ± 0.004	63.1 ± 0.3
Tanh, sTanh	0.015 ± 0.003	67.2 ± 0.3
Tanhshrink, sTanh	0.027 ± 0.006	45.2 ± 0.2
SiLU, Kaiming	0.031 ± 0.008	57.1 ± 2.5
sTanh, Kaiming	0.041 ± 0.019	60.3 ± 2.5
Tanh, Kaiming	0.050 ± 0.022	58.5 ± 2.3
Tanhshrink, Kaiming	0.082 ± 0.014	38.7 ± 1.8

Balanced Extended MNIST

To show that the NEAR score can be utilized to guide the selection of the activation function and weight initialization scheme across various datasets and independent of the optimizer, we report the test loss and the NEAR

score on the balanced EMNIST dataset. We employed a multi-layer perceptron with two hidden layers of size 200 in combination with the Adam optimizer [58]. We applied early stopping with a patience of 10 epochs, whereby 10% of the training set served as validation set.

We report the test loss and the NEAR score for the initialization schemes Xavier uniform [22], Kaiming uniform, and uniform and the activation functions SiLU, ReLU, Tanh, and Tanhshrink in Table 10. The NEAR score indicates that the Xavier initialization is the most effective, followed by the Kaiming initialization and the uniform initialization. While the uniform initialization is undoubtedly the least favorable in terms of resulting test loss, the distinction between Xavier and Kaiming is not as clear-cut. For the activation functions under consideration, the average loss is found to be lower with the Kaiming initialization than the Xavier initialization, but the difference is marginal and the standard deviations are higher than the difference.

For the Kaiming and Xavier initializations, the activation functions SiLU, ReLU, and Tanh result in similar test losses, while the NEAR score gives the impression that there is a clear ordering for a given initialization. As the orderings of the test losses and NEAR scores do not agree for both initializations, we conclude that these small differences in the resulting loss cannot be captured by the NEAR score. We note here again that the NEAR score only accounts for the expressivity of the network and does not take into account the training process. Still, the NEAR score can reliably predict the worst performing activation function (Tanhshrink). For this activation function, the test loss is also significantly different from those of the others. Analogously, the NEAR score can correctly identify that SiLU, Tanhshrink, and ReLU lead to a lower loss than Tanh if the uniform initialization is applied. Hence, NEAR is able to predict whether an activation function and weight initialization scheme performs well or bad, and only small differences in the resulting loss are not resolved.

5. CONCLUSION

In this work, we have introduced NEAR which is a zero-cost proxy to pre-estimate the performance of a machine learning model without training. For this purpose, the NEAR score estimates the expressivity of neural networks by calculating the effective rank of the pre- and post-activation matrix. We have demonstrated its strong correlation with the final model accuracy on NATS-Bench-SSS/TSS and NAS-Bench-101. In a ranking of 13 zero-cost proxies by their Spearman’s correlation coefficient, NEAR achieves an average rank of 1.7 across all datasets and search spaces, while the second-best proxy MeCo_{opt} has only an average rank of 2.6. In contrast to other proxies, NEAR only requires sample input data, but no output labels and it is not bound to a specific activation function. In fact, we have shown that it can even

Table 10: Comparison of the test loss (after training) and the NEAR score (before training) for various activation functions σ and weight initialization schemes on the balanced EMNIST dataset. The table is sorted by ascending test loss. All experiments were repeated 20 times with different randomly initialized neural networks and a random selection of inputs employed to calculate the NEAR score in each repetition. We report the mean and the standard deviation (rounded up). For “SiLU, uniform” one outlier was excluded from the mean and standard deviation.

σ , initialization	Test loss	NEAR score
SiLU, Kaiming	0.367 ± 0.008	382.8 ± 5.0
SiLU, Xavier	0.368 ± 0.008	417.7 ± 0.6
ReLU, Kaiming	0.372 ± 0.010	403.7 ± 7.4
ReLU, Xavier	0.374 ± 0.008	421.1 ± 0.8
Tanh, Kaiming	0.392 ± 0.010	398.2 ± 5.1
Tanh, Xavier	0.396 ± 0.011	415.5 ± 0.4
Tanhshrink, Kaiming	0.447 ± 0.022	278.4 ± 3.2
Tanhshrink, Xavier	0.449 ± 0.018	401.4 ± 1.2
SiLU, uniform	0.525 ± 0.040	13.3 ± 0.1
Tanhshrink, uniform	0.602 ± 0.030	13.4 ± 0.1
ReLU, uniform	0.651 ± 0.047	13.3 ± 0.1
Tanh, uniform	3.858 ± 0.030	9.0 ± 0.1

be applied to choose a well performing activation function and weight initialization scheme. Moreover, NEAR is not limited to a given search space and can be applied to estimate the optimal layer size in multi-layer perceptrons. This task represents a significant challenge in the construction of neural networks, and hence, NEAR can help substantially reduce invested human time and computational demand.

CODE AVAILABILITY

The NEAR software is available on GitHub (<https://github.com/ReiherGroup/NEAR>).

ACKNOWLEDGMENTS

This work was created as part of NCCR Catalysis (grant number 180544), a National Centre of Competence in Research funded by the Swiss National Science Foundation. M.E. was supported by an ETH Zurich Postdoctoral Fellowship.

-
- [1] C. M. Bishop, *Pattern Recognition and Machine Learning* (Springer, New York, NY, USA, 2006).
- [2] S. Russell and P. Norvig, *Artificial Intelligence: A Modern Approach*, 4th ed. (Pearson, Harlow, United Kingdom, 2021).
- [3] A. Vaswani, N. Shazeer, N. Parmar, J. Uszkoreit, L. Jones, A. N. Gomez, Ł. Kaiser, and I. Polosukhin, Attention is all you need, in *Adv. Neural Inf. Process. Syst.*, Vol. 30 (2017).
- [4] A. Baevski, Y. Zhou, A. Mohamed, and M. Auli, wav2vec 2.0: A framework for self-supervised learning of speech representations, in *Adv. Neural Inf. Process. Syst.*, Vol. 33 (2020) pp. 12449–12460.
- [5] J. Jumper, R. Evans, A. Pritzel, T. Green, M. Figurnov, O. Ronneberger, K. Tunyasuvunakool, R. Bates, A. Žídek, A. Potapenko, *et al.*, Highly accurate protein structure prediction with AlphaFold, *Nature* **596**, 583 (2021).
- [6] K. Hornik, M. Stinchcombe, and H. White, Multilayer feedforward networks are universal approximators, *Neural Netw.* **2**, 359 (1989).
- [7] G. Cybenko, Approximation by superpositions of a sigmoidal function, *Math. Control Signals Syst.* **2**, 303 (1989).
- [8] K. Hornik, Approximation capabilities of multilayer feedforward networks, *Neural Netw.* **4**, 251 (1991).
- [9] M. Tan and Q. Le, EfficientNet: Rethinking model scaling for convolutional neural networks, in *36th International Conference on Machine Learning (ICML)* (Long Beach, United States of America, 2019) pp. 6105–6114.
- [10] P. Ren, Y. Xiao, X. Chang, P.-Y. Huang, Z. Li, X. Chen, and X. Wang, A comprehensive survey of neural architecture search: Challenges and solutions, *ACM Comput. Surv.* **54**, 1 (2021).
- [11] T. Elsken, J. H. Metzen, and F. Hutter, Neural architecture search: A survey, *J. Mach. Learn. Res.* **20**, 1 (2019).
- [12] B. Zoph and Q. V. Le, Neural architecture search with reinforcement learning, in *5th International Conference on Learning Representations (ICLR)* (Toulon, France, 2017).
- [13] E. Real, S. Moore, A. Selle, S. Saxena, Y. L. Suematsu, J. Tan, Q. V. Le, and A. Kurakin, Large-scale evolution of image classifiers, in *34th International Conference on Machine Learning (ICML)* (Sydney, Australia, 2017) pp. 2902–2911.
- [14] H. Liu, K. Simonyan, and Y. Yang, DARTS: Differentiable architecture search, in *7th International Conference on Learning Representations (ICLR)* (New Orleans, United States of America, 2019).
- [15] J. Mellor, J. Turner, A. Storkey, and E. J. Crowley, Neural architecture search without training, in *38th International Conference on Machine Learning (ICML)* (2021) pp. 7588–7598.
- [16] M. S. Abdelfattah, A. Mehrotra, Ł. Dudziak, and N. D. Lane, Zero-cost proxies for lightweight NAS, in *9th International Conference on Learning Representations (ICLR)* (2021).
- [17] A. Krishnakumar, C. White, A. Zela, R. Tu, M. Safari, and F. Hutter, NAS-Bench-Suite-Zero: Accelerating research on zero cost proxies, in *Adv. Neural Inf. Process. Syst.*, Vol. 35 (2022) pp. 28037–28051.
- [18] X. Ning, C. Tang, W. Li, Z. Zhou, S. Liang, H. Yang, and Y. Wang, Evaluating efficient performance estimators of neural architectures, in *Adv. Neural Inf. Process. Syst.*, Vol. 34 (2021) pp. 12265–12277.

- [19] J. Behler and M. Parrinello, Generalized neural-network representation of high-dimensional potential-energy surfaces, *Phys. Rev. Lett.* **98**, 146401 (2007).
- [20] J. Behler, Four generations of high-dimensional neural network potentials, *Chem. Rev.* **121**, 10037 (2021).
- [21] Y. LeCun, L. Bottou, G. B. Orr, and K.-R. Müller, Efficient backprop, in *Neural networks: Tricks of the trade* (Springer Berlin Heidelberg, 1998) pp. 9–50.
- [22] X. Glorot and Y. Bengio, Understanding the difficulty of training deep feedforward neural networks, in *13th International Conference on Artificial Intelligence and Statistics (AISTATS)* (Sardinia, Italy, 2010) pp. 249–256.
- [23] J. Snoek, H. Larochelle, and R. P. Adams, Practical bayesian optimization of machine learning algorithms, in *Adv. Neural Inf. Process. Syst.*, Vol. 25 (2012).
- [24] P. R. Lorenzo, J. Nalepa, M. Kawulok, L. S. Ramos, and J. R. Pastor, Particle swarm optimization for hyperparameter selection in deep neural networks, in *Genetic and Evolutionary Computation Conference* (Berlin, Germany, 2017) pp. 481–488.
- [25] O. Roy and M. Vetterli, The effective rank: A measure of effective dimensionality, in *15th European signal processing conference* (2007) pp. 606–610.
- [26] N. Lee, T. Ajanthan, and P. H. Torr, SNIP: Single-shot network pruning based on connection sensitivity, in *7th International Conference on Learning Representations (ICLR)* (New Orleans, United States of America, 2019).
- [27] C. Wang, G. Zhang, and R. Grosse, Picking winning tickets before training by preserving gradient flow, in *8th International Conference on Learning Representations (ICLR)* (Addis Ababa, Ethiopia, 2020).
- [28] J. Turner, E. J. Crowley, M. O’Boyle, A. Storkey, and G. Gray, BlockSwap: Fisher-guided block substitution for network compression on a budget, in *8th International Conference on Learning Representations (ICLR)* (Addis Ababa, Ethiopia, 2020).
- [29] H. Tanaka, D. Kuzin, D. L. Yamins, and S. Ganguli, Pruning neural networks without any data by iteratively conserving synaptic flow, in *Adv. Neural Inf. Process. Syst.*, Vol. 33 (2020) pp. 6377–6389.
- [30] G. Li, Y. Yang, K. Bhardwaj, and R. Marculescu, ZiCo: Zero-shot NAS via inverse coefficient of variation on gradients, in *11th International Conference on Learning Representations (ICLR)* (Kigali, Rwanda, 2023).
- [31] M. Lin, P. Wang, Z. Sun, H. Chen, X. Sun, Q. Qian, H. Li, and R. Jin, Zen-NAS: A zero-shot NAS for high-performance image recognition, in *Proc. IEEE Int. Conf. Comput. Vis.* (2021) pp. 347–356.
- [32] Y. Peng, A. Song, H. M. Fayek, V. Ciesielski, and X. Chang, SWAP-NAS: Sample-wise activation patterns for ultra-fast NAS, in *12th International Conference on Learning Representations (ICLR)* (Vienna, Austria, 2024).
- [33] T. Jiang, H. Wang, and R. Bie, MeCo: Zero-shot NAS with one data and single forward pass via minimum eigenvalue of correlation, in *Adv. Neural Inf. Process. Syst.*, Vol. 36 (2023) pp. 61020–61047.
- [34] W. Chen, X. Gong, and Z. Wang, Neural architecture search on ImageNet in four GPU hours: A theoretically inspired perspective, in *9th International Conference on Learning Representations (ICLR)* (2021).
- [35] V. Nair and G. E. Hinton, Rectified linear units improve restricted boltzmann machines, in *27th International Conference on Machine Learning (ICML)* (Haifa, Israel, 2010) pp. 807–814.
- [36] R. Pascanu, G. Montufar, and Y. Bengio, On the number of inference regions of deep feed forward networks with piece-wise linear activations, in *2nd International Conference on Learning Representations (ICLR)* (Banff National Park, Canada, 2013).
- [37] G. F. Montufar, R. Pascanu, K. Cho, and Y. Bengio, On the number of linear regions of deep neural networks, in *Adv. Neural Inf. Process. Syst.*, Vol. 27 (2014).
- [38] M. Raghu, B. Poole, J. Kleinberg, S. Ganguli, and J. Sohl-Dickstein, On the expressive power of deep neural networks, in *34th International Conference on Machine Learning (ICML)* (Sydney, Australia, 2017) pp. 2847–2854.
- [39] G. Montúfar, Notes on the number of linear regions of deep neural networks, in *12th International Conference on Sampling Theory and Applications (SampTA)* (Tallinn, Estonia, 2017).
- [40] T. Serra, C. Tjandraatmadja, and S. Ramalingam, Bounding and counting linear regions of deep neural networks, in *35th International Conference on Machine Learning (ICML)* (Stockholm, Sweden, 2018) pp. 4558–4566.
- [41] C. E. Shannon, A mathematical theory of communication, *Bell Syst. Tech. J.* **27**, 379 (1948).
- [42] Z. Li, F. Liu, W. Yang, S. Peng, and J. Zhou, A survey of convolutional neural networks: analysis, applications, and prospects, *IEEE Trans. Neural Netw. Learn. Syst.* **33**, 6999 (2021).
- [43] C. Ying, A. Klein, E. Christiansen, E. Real, K. Murphy, and F. Hutter, NAS-Bench-101: Towards reproducible neural architecture search, in *36th International Conference on Machine Learning (ICML)* (Long Beach, United States of America, 2019) pp. 7105–7114.
- [44] X. Dong, L. Liu, K. Musial, and B. Gabrys, NATS-Bench: Benchmarking NAS algorithms for architecture topology and size, *IEEE Trans. Pattern Anal. Mach. Intell.* **44**, 3634 (2021).
- [45] M. G. Kendall, A new measure of rank correlation, *Biometrika* **30**, 81 (1938).
- [46] C. Spearman, The proof and measurement of association between two things., *Am. J. Psychol.* **15**, 72 (1904).
- [47] R. T. Husstein, M. Reiher, and M. Eckhoff, NEAR: A training-free pre-estimator of machine learning model performance (version 1.0), Zenodo 10.5281/zenodo.13332011 (2024).
- [48] A. Krizhevsky and G. Hinton, *Learning multiple layers of features from tiny images*, Tech. Rep. (University of Toronto, 2009).
- [49] P. Chrabaszcz, I. Loshchilov, and F. Hutter, A downsampled variant of imagenet as an alternative to the CIFAR datasets, arXiv:1707.08819 [cs.CV] (2017).
- [50] J. Kaplan, S. McCandlish, T. Henighan, T. B. Brown, B. Chess, R. Child, S. Gray, A. Radford, J. Wu, and D. Amodei, Scaling laws for neural language models, arXiv:2001.08361 [cs.LG] (2020).
- [51] G. Cohen, S. Afshar, J. Tapson, and A. van Schaik, EMNIST: Extending MNIST to handwritten letters, in *International Joint Conference on Neural Networks (IJCNN)* (IEEE, Anchorage, United States of America, 2017) pp. 2921–2926.
- [52] Y. LeCun, L. Bottou, Y. Bengio, and P. Haffner, Gradient-based learning applied to document recogni-

- tion, *Proc. IEEE* **86**, 2278 (1998).
- [53] M. Eckhoff and M. Reiher, Lifelong machine learning potentials, *J. Chem. Theory Comput.* **19**, 3509 (2023).
- [54] M. Eckhoff and M. Reiher, CoRe optimizer: an all-in-one solution for machine learning, *Mach. Learn.: Sci. Technol.* **5**, 015018 (2024).
- [55] M. Eckhoff and M. Reiher, Reiher-Group/CoRe_optimizer: Release 1.1.0, Zenodo 10.5281/zenodo.11551858 (2024).
- [56] K. He, X. Zhang, S. Ren, and J. Sun, Delving deep into rectifiers: Surpassing human-level performance on imagenet classification, in *Proc. IEEE Int. Conf. Comput. Vis.* (2015) pp. 1026–1034.
- [57] S. Elfving, E. Uchibe, and K. Doya, Sigmoid-weighted linear units for neural network function approximation in reinforcement learning, *Neural Netw.* **107**, 3 (2018).
- [58] D. P. Kingma and J. Ba, Adam: A method for stochastic optimization, in *3rd International Conference on Learning Representations ICLR* (San Diego, United States of America, 2015).